Catalysis Today 427 (2024) 114419

Contents lists available at ScienceDirect

Catalysis Today

journal homepage: www.elsevier.com/locate/cattod

Catalytic upgrading of lignin-derived bio-oils over ion-exchanged H-ZSM-5 and H-beta zeolites

M.I. Ávila [a], M.M. Alonso-Doncel [b], L. Briones [a], G. Gómez-Pozuelo [a], J.M. Escola [a], D. P. Serrano [a,b], A. Peral [a], J.A. Botas [a,*]

[a] Chemical and Environmental Engineering Group, ESCET, Rey Juan Carlos University, c/ Tulipán s/n, 28933 Móstoles, Madrid, Spain
[b] Thermochemical Processes Unit, IMDEA Energy, Avda. Ramón de la Sagra 3, 28935, Móstoles, Madrid, Spain

ARTICLE INFO

Keywords:
Lignin pyrolysis
H-ZSM-5
H-Beta
Ion-exchanged zeolites
Oxygenated aromatics

ABSTRACT

H-ZSM-5 and H-Beta zeolites ion-exchanged with alkali (Na^+ and K^+) and alkaline-earth (Mg^{2+}) metals have been explored for the catalytic fast pyrolysis of lignin. Incorporating these metals led to a significant change in the acidic properties of the parent zeolites turning into mostly Lewis-type acidity. Catalytic fast pyrolysis experiments of lignin were performed in a fixed bed reactor with ex-situ configuration operating at 550 °C (thermal zone) and 450 °C (catalytic zone), atmospheric pressure and under a nitrogen flow. Moreover, two catalysts to lignin mass ratios (C/L = 0.2 and 0.4) were studied. Compared with non-catalytic tests, the use of parent zeolites caused a decrease in the bio-oil* (water-free basis) yield due to enhanced production of gases, water, and the coke deposition on the catalyst. In addition, the quality of bio-oil* was improved since it presents a lower oxygen content regarding the thermal test. H-Beta zeolite showed a higher deoxygenation degree than H-ZSM-5, but the latter exhibited a higher share of light components in the bio-oil* that can be detected by GC-MS analyses. Both catalysts promoted the production of light oxygenates, aromatics, and oxygenated aromatics. Regarding the effect of the incorporation of metals, oxygenated aromatic compounds were the predominant family in the bio-oil* obtained with all ion-exchanged zeolites. Likewise, significant differences were observed among the catalysts regarding the main components of this family (alkylphenols, guaiacols, syringols, catechols, and methoxybenzenes), achieving guaiacols concentrations in bio-oil* near to 24 wt.% for NaH-ZSM-5 and KH-ZSM-5 catalysts, and alkylphenols concentrations close to 16 wt.% for MgH-Beta and KH-Beta zeolites.

1. Introduction

There is a worldwide need to develop sustainable routes for the production of chemicals replacing fossil fuels as feedstock. In this regard, lignocellulosic biomass, which is made up of three components (cellulose, hemicellulose and lignin), has become an interesting and renewable raw material. Around 120–130 million tonnes of residual biomass are generated annually from agriculture, forestry, and industry refuse [1]. These data evidence the great potential of lignocellulose for the production of both advanced biofuels and bio-based chemicals, according to the biorefinery approach. Thus, lignocellulosic biomass may efficiently substitute fossil fuels as a source of many commonplace chemicals in everyday life [2].

One of the major components of lignocellulosic biomass is lignin, whose share varies depending on the biomass nature (25 – 31 wt.% in softwoods, 16 – 24 wt.% in hardwoods, and 16 – 21 wt.% in herbaceous crops). Lignin is obtained in a great deal as a by-product in the paper mill industry, and it is typically employed for heat generation by burning [3–6]. However, lignin is a polymer made up of several building blocks named monolignols (e.g. sinapyl alcohol (S), coniferyl alcohol (G), and p-coumaryl alcohol (H)), which may be harnessed for obtaining different phenolic compounds with commercial applications, in keeping with the biorefinery approach. The content of these monolignols depends on the kind of biomass since the percentage of S monolignols is around 95% in softwood lignin, while hardwood lignin contains S and G units, and herbaceous crops present the three of them (S, G and H). These units are joined using C-O-C (β-O-4, α-O-4 and 4-O-5) and C-C (5–5, β-β, β-5 and β-1) linkages, being the most abundant the β-O-4. The latter linkage is particularly important since it has been proven to determine the yield of alkylphenols during the catalytic depolymerisation of lignin [7]. In addition, the particular makeup of lignin is a key factor in its further upgrading. Thus, a relationship has been found

* Corresponding author.
E-mail address: juanangel.botas@urjc.es (J.A. Botas).

https://doi.org/10.1016/j.cattod.2023.114419
Received 15 July 2023; Received in revised form 6 October 2023; Accepted 16 October 2023
Available online 20 October 2023

between the formation of oligomers and monophenols in the lignin pyrolysis process and the respective lignin structure (e.g., alkali lignin or corn cob hydrolysis residue lignin), which has been ascribed to its different content of G units [8].

In order to obtain valuable chemicals from lignin, it has to be depolymerised. There are different alternatives for doing so: pyrolysis, solvolysis, catalytic oxidative depolymerisation, and catalytic reductive polymerisation [6,8]. Before depolymerising, it is recommended to isolate the lignin from the holocellulose to avoid inconvenient downstream separation processes to attain the desired bulk chemicals. A clear advantage of pyrolysis is its technical simplicity. Pyrolysis consists of the thermal treatment in the absence of oxygen at temperatures between 300 and 700 °C [9], which decomposes the lignin into gases, bio-oil and biochar. Depending on the operation conditions (temperature, residence time and heating rate), pyrolysis is classified into slow, fast and flash. Fast pyrolysis with high heating rates, temperatures within 400–600 °C and short residence times enables to maximise the yield of bio-oil (up to 50–55%). This bio-oil poses several problems, such as its instability, corrosive nature and low heating value [10], and it is usually made up of a broad diversity of components that makes difficult to leverage it for obtaining specific chemicals.

Catalytic fast pyrolysis (CFP) of lignin has appeared as a promising route to enhance the production of valuable chemicals, and a variety of catalysts has been tested: molecular sieves catalysts, clay minerals and industrial solid wastes, metal salts and metal oxides [11]. In this regard, new mixed metal oxides (WO_x-TiO_2-Al_2O_3) have proven to be efficient solid Lewis acid catalysts for producing aromatics by lignin pyrolysis [12].

Zeolites have been applied in the catalytic pyrolysis of lignin, although they are usually quickly deactivated by coke deposition. Thus, catalytic fast pyrolysis of soda lignin was investigated over three zeolites (Y, mordenite and ZSM-5) differing in pore size and Si/Al atomic ratio (acidity) within the 500–900 °C temperature range. It was found that zeolite Y was the most suitable catalyst for the demethoxylation and dehydroxylation of bulky oxygenates towards phenolics and especially aromatic dimers, because of its larger pore size [13]. On the other hand, mesoporous aluminosilicates (Al-MCM-41, Al-SBA-15 and Al-MSU-J) gave rise in the catalytic fast pyrolysis of lignin to chiefly aromatics and phenolics due to both its enhanced accessibility and mild acidity, preferentially of Lewis nature [14]. The acidity of aluminium-containing zeolites can be modulated by ion-exchange with cationic metals. Thus, their acidic features, caused by the presence of both Brønsted and Lewis acid sites of different strength, can be adjusted generating catalysts with a higher proportion of Lewis acid sites and an interesting combination of acid-base properties that improve their performance in different catalysis and adsorption processes [15–17]. A variety of metal-modified zeolites have been applied in lignin valorisation by catalytic pyrolysis, MFI, BEA, FAU and MOR being some of the zeolite structures more studied. Pore size, pore structure and acidity impact clearly on the selectivity and the amount of coke produced [11].

In previous works of our group, we reported an enhanced selectivity towards oxygenated aromatics (phenols, alkylphenols) over nanocrystalline KH-ZSM-5 and K-USY catalysts in the catalytic pyrolysis of wheat straw due to its right combination of acid-base properties and good accessibility [18,19]. The present work aims to upgrade the vapours from lignin thermal pyrolysis over both acid-form H-ZSM-5 and H-Beta zeolites exchanged with different cations (Na^+, K^+ and Mg^{2+}). In this respect, the suitable tuning of their acid/base properties by an ion-exchange procedure is aimed at obtaining valuable phenolic compounds. Herein, the obtained results are reported.

2. Experimental procedures

2.1. Catalysts samples

Two different types of commercial zeolites in their acid-form were kindly provided by Clariant, with MFI (CZP 90) and BEA (CZB 30) structures. In this work, these samples are referred to as H-ZSM-5 and H-Beta, respectively. Besides being tested in reaction as acid catalysts, both zeolites were also the parent materials for preparing other catalysts by ion exchange. In this way, the as-received samples were firstly dried and then ion-exchanged with alkali (Na^+ and K^+) and alkaline-earth (Mg^{2+}) cations following procedures previously described in the literature [15,18]. Typically, the zeolite powder (5 g) was soaked into 50 ml of a 0.4 M aqueous solution of the appropriate chlorine salt for 24 h at 25 °C. NaCl (99.0 wt.%, Sigma Aldrich), KCl (99.0 wt.%, Scharlab), and $MgCl_2$ (99.0 wt.%, Fisher Scientific) were used as salts for the ion-exchange. Subsequently, the ion-exchanged zeolites were recovered by centrifugation, washed with Mili-Q water, dried in an oven overnight at 110 °C and, finally, calcined in static air (550 °C, 5 h, heating rate of 1.8 °C/min). Previously to their use as catalysts in reaction, the zeolite samples were pelletised under pressure (8 tons, 30 s), crushed, and sieved to the desired particle size (180–250 μm).

2.1.1. Catalysts characterisation

The aluminium and metal content of the different catalysts were determined by using inductively coupled plasma-optical emission spectroscopy (ICP-OES) with a Varian Vista AX spectrometer. Previously to the measurements, the samples were digested in an acid H_2SO_4/HF solution. X-ray diffraction (XRD) patterns were obtained using a Philips X'pert diffractometer with Cu Kα radiation. Ar adsorption-desorption isotherms of the different samples were collected employing a Micromeritics 3Flex Adsorption Analyzer. Prior to the analysis, the samples were outgassed at 300 °C under vacuum for 5 h. The Brunauer-Emmet-Teller (BET) equation was used to determine the BET surface area. The t-plot method was used to evaluate the contribution of micro-mesopores to the overall surface area. The total pore volume was calculated based on the amount adsorbed at a relative pressure of 0.95. Transmission electron microscopy (TEM) images, along with energy-dispersive X-ray (EDX) analyses, were performed by using a JEOL JEM1400-Flash microscope operating at 120 kV.

The nature and strength of the acid sites in the zeolites were investigated using pyridine adsorption/desorption followed by Fourier transform infrared spectroscopy (FTIR/PYR) tests. Self-supporting wafer samples were firstly prepared (8–15 mg/cm^2) and loaded into a High Temperature Cell (HTC) provided with CaF_2 window. Activation was performed under vacuum at 525 °C for 1 h. After activation, pyridine adsorption occurred at 150 °C and 4 mbar pressure, and FTIR spectra were recorded in the 4000–400 cm^{-1} range (4 cm^{-1} resolution and 128 scans). A Jasco FT/IR-4600 provided with a triglycine sulfate (TGS) detector was used for the latter purpose. Additionally, the FTIR spectra were recorded after pyridine evacuation at different desorption temperatures (150, 250, 350, and 450 °C) to evaluate the strength of acid sites. The quantification of acid sites was performed using specific pyridine vibration modes and absorption coefficients, which can be found in the literature [20]: pyridinium PyH^+ band at 1545 cm^{-1} ($\varepsilon_{H\text{-}ZSM\text{-}5}$=1.09 cm/μmol; $\varepsilon_{H\text{-}Beta}$=1.12 cm/μmol) and pyridine PyL band at ~1455 cm^{-1} ($\varepsilon_{H\text{-}ZSM\text{-}5\ and\ H\text{-}Beta}$=1.71 cm/μmol; $\varepsilon_{MeH\text{-}ZSM\text{-}5\ and\ MeH\ \text{-}Beta}$=1.72 cm/μmol).

Additionally, temperature-programmed desorption of carbon dioxide (CO_2-TPD) analyses were carried out using a Micromeritics Autochem 2930 equipment aiming to determine the basic properties of the catalysts. CO_2-TPD involved degassing the catalyst sample at 550 °C for 2 h, followed by CO_2 saturation at 50 °C using a 5% CO_2/He mixture for 30 min and purged at 50 °C for 45 min under He flow. CO_2-TPD profiles were recorded by increasing the temperature under He flow from 50 °C to 550 °C with a temperature ramp rate of 10 °C/min.

2.2. Lignin feedstock

The selected lignin to be processed in the pyrolysis tests was Tanovis Protobind 1000, supplied by PLT Innovations in powder form, which is

obtained from non-woody biomass according to the Soda process extraction [21].

Prior to the pyrolysis tests, the lignin was conformed into tablets of uniform size, shape, and weight, using a hydraulic press and a force of 8 tons for 30 s. Afterwards, the pills were crushed and screened through ASTM standard sieves to reach the desired grain size to feed the pyrolysis reactor (0.5 – 1 mm). Finally, the milled lignin was dried in an oven at 105 °C to remove the moisture.

2.2.1. Lignin characterisation

The lignin employed as feedstock in the pyrolysis tests was characterised following the European Standards UNE-EN ISO 18134–1:2016, UNE-EN ISO 18123:2016 and UNE-EN ISO 18122:2016 to obtain its moisture, ash, and volatile matter contents, respectively. Concretely, the moisture was calculated through the lignin total weight loss after treatment in an oven at 105 °C overnight. Ash content was the residual mass obtained after the calcination of dry lignin in a muffle oven at 900 °C (heating rate of 1.8 °C/min) with an isotherm step of 30 min. Volatile matter (VM) was determined by thermogravimetric analysis using a thermobalance TA instrument SDT 650, heating up the sample to 900 °C at 10 °C/min and maintaining this temperature for 30 min under inert atmosphere (100 ml/min of N_2). The total weight loss so-obtained was assigned to the volatile matter, and the fixed carbon (FC) was estimated by difference employing Eq. 1.

$$\text{FC}\ \ (\text{wt.\%}) = 100 - \text{VM}\ (\text{wt.\%}) - \text{Ash}\ \ (\text{wt.\%}) \tag{1}$$

Ultimate analysis, i.e., the lignin proportions in carbon (C), hydrogen (H), nitrogen (N) and sulphur (S), expressed in wt.%, were directly measured using a ThermoFisher Flash Smart micro-elemental analyser, being the oxygen (O) content calculated by difference. The higher heating value (HHV) was determined by employing the following (Eq. 2) empirical correlation [22], where A refers to the ash content of lignin (wt.%).

$$\text{HHV}\left(\frac{\text{MJ}}{\text{kg}}\right) = 0.3491\cdot\text{C} + 1.1783\cdot\text{H} + 0.1005\cdot\text{S} - 0.1034\cdot\text{O} - 0.0151\cdot\text{N} - 0.211\cdot\text{A} \tag{2}$$

ATR-FTIR spectra were obtained on a Nicolet iS-50 spectrometer. Measurements were carried out using lignin powder, and spectra were recorded over the range from 4000 to 500 cm^{-1} at a resolution of 2 $cm^{-1,}$ while 64 scans were averaged to reduce noise.

2.3. Lignin pyrolysis tests

The lignin pyrolysis tests were carried out in a downflow fixed-bed stainless steel reactor (16 mm inner diameter and 400 mm length) with independent thermal and catalytic zones heated by two electrical furnaces. The reaction temperatures are controlled by type K thermocouples located in both zones. In all the reactions, the amount of lignin employed as feedstock was 4 g, and for the catalytic tests, the catalyst to lignin mass ratio (C/L) was 0.2 and 0.4. The lignin was fed with a particle size ranging from 0.5 to 1 mm, and the catalysts were deposited in the respective reactor zone with a particle size between 180 and 250 μm. The operation conditions were atmospheric pressure and temperatures of 550 °C and 450 °C for the thermal and catalytic zones, respectively. Before each experiment, the biomass tank and the reaction system are purged with 100 ml/min of nitrogen. Once the thermal and catalytic pyrolysis zones reach the desired temperatures, the biomass is loaded into the reactor, and the pyrolysis of lignin is performed for 10 min by feeding a constant flow of 100 ml/min of nitrogen. Thus, the lignin is decomposed into carbonaceous residue or char (thermal zone), non-condensable gases and pyrolytic vapours, which pass through the catalytic zone. The vapours leaving the reactors are condensed through a system of two stainless steel vessels refrigerated by an ice-water bath. The non-condensable gases are collected for further analysis in a totaliser, which also allows the measurement of the gas volume by water displacement. Finally, after the reaction tests, gases, char (accumulated in the thermal zone), coke (deposited over the catalyst) and bio-oil are characterised by means of different analytical techniques. A detailed scheme of the experimental set-up can be found in a previous work [23].

2.3.1. Analysis of the lignin pyrolysis products

The condensed bio-oil in the catalytic pyrolysis tests consists of two phases (aqueous and organic-rich), which were separated by decantation. The water content of each phase was quantified by Karl Fischer titration following ASTM E202–08 procedure. Moreover, the composition of C, H, N and S of both phases was measured employing a ThermoFisher Flash Smart micro-elemental analyser, and the oxygen content was calculated by difference. The organic components present in the two liquid phases (named as bio-oil*, on a water-free basis) were obtained employing a gas chromatograph coupled with a mass spectrometer detector (GC-MS) Bruker® SCION 436-GC (electron energy: 70 eV; Emission: 300 V; He flow rate: 1 ml/min; Column: WCOT fused silica HP5-MS UI (30 m × 0.25 mm × 0.25 mm). The bio-oil* products were identified by comparison with the NIST EI-MS spectral library (v.2.0), considering a minimum match score of 700. Once identified, the compounds were grouped into different families according to their main functional groups: carboxylic acids (CA), light oxygenates (LO, including aldehydes, alcohols, ketones and ethers), furans (FUR), oxygenated aromatics (O-AR) and aromatic hydrocarbons (AR). In order to obtain a quantitative analysis, an external calibration was carried out using a total of 19 compounds, which are present in either thermal and catalytic bio-oils: acetic acid, propanoic acid, butanone, diethoxy propane, cyclopentenone, furfural, phenol, guaiacol, cresol, dimethylphenol, creosol, syringol, trimethoxybenzene, toluene, xylene, styrene, trimethylbenzene, naphthalene and n-heptane. The response factors of the rest of the detected compounds were estimated as the average of their corresponding group. The difference between the overall and GC-MS detected bio-oil yields allows the estimation of GC-MS non-detected components, which correspond with heavy/oligomeric species.

Non-condensable gases were analysed in a Varian CP-4900 micro gas chromatograph with two columns: Molsieve 5 Å and PPQ, and a thermal conductivity detector (TCD), using argon and helium as the carrier gas, respectively. In order to quantify the gases content, the equipment was calibrated employing standard gas mixtures of N_2, O_2, H_2, CO, CO_2, CH_4, C_2H_4, C_2H_6, C_3H_6, C_3H_8, C_4H_8 and C_4H_{10}.

The C, H, N, S and O contents in the char and coke were measured employing a ThermoFisher Flash Smart micro-elemental analyser.

The amount of coke deposited over the catalyst was calculated by TPO measurements under air atmosphere using a TA instrument SDT 650 thermobalance (up 900 °C and a heating rate of 10 °C/min).

Finally, the total mass balance was closed within > 95 wt.% from the weight of the gas, bio-oil, char and coke fractions.

Table 1
Proximate and ultimate analyses of lignin.

Proximate analysis[a] (wt.%)			Ultimate analysis[b] (wt.%)					HHV[d] (MJ/kg)
Volatile matter	Ash	Fixed carbon	C	H	N	S	O[c]	
61.7	1.3	37.0	60.0	5.2	0.7	0.4	33.7	23.3

[a] Dry basis
[b] Dry ash-free basis
[c] Determined by difference
[d] Higher Heating Value

3. Results and discussion

3.1. Lignin characterisation

The results of proximate and ultimate analyses of lignin are shown in Table 1. Compared with typical values obtained for lignocellulosic biomass, lignin exhibits lower volatile matter and oxygen contents and higher fixed carbon and high heating value [24]. The C, H, N and O content are typical for lignin samples [25], while the sulphur content depends on the extraction method of lignin and the raw biomass selected. In the lignin chosen in this work, the sulphur may come from the sulphuric acid used for the neutralisation step required for lignin precipitation in the extraction step of Soda method. On the other hand, the ash content and its composition are related to the extraction method and the raw biomass composition. Protobind 1000 lignin proceeded from straw and grass that contain more minerals per dry weight than woody biomass [4].

Regarding its structure, lignin is a heterogeneous and three-dimensional polymer formed by three monomers: p-coumaryl, coniferyl and sinapyl alcohol. The phenolic compounds derived from these alcoholic monomers are known as p-hydroxyphenyl (derived from coumaryl alcohol), guaiacyl (from coniferyl alcohol) and syringyl (from sinapyl monomer), whose proportions depend on the type of biomass chosen to extract the lignin. In addition, other oxygen-containing functional groups can be found in lignin, such as methoxy, carbonyl and hydroxyl groups, increasing the complexity of its structure [2,3,26]. Therefore, lignin decomposition is a complex mechanism that is performed through several competitive reactions, and this has been studied through thermogravimetry under nitrogen atmosphere, which is represented in Fig. 1. During its thermal degradation, various cleavages within lignin molecules occur over a wide temperature, with the main decompositions being observed between 200 and 700 °C [27–29]. In this temperature range, the dehydration stage occurs at low temperatures (< 150 °C), followed by the degradation attributed to the cleavage of poorly thermally stable β-O-4 linkages (200 – 400 °C) [30]. Finally, the decomposition and carbonisation of the remaining lignin occur (> 500 °C) [26], with the degradation of lignosulphonates and also the polymerisation of lignin to form char, obtaining a final residue of 37 wt. % [31]. It is important to highlight that Protobind-type lignin usually contains residual carbohydrates (about 4 wt.%), which degrade around 250 °C [4], as confirmed by the corresponding signal at that temperature observed in the DTG curve of Fig. 1. According to literature, below 400 °C, the lignin decomposition occurs mainly by forming water and formaldehyde due to the break of methyl-aryl ether bonds [32]. The most abundant product is water derived from the abundant hydroxyl and methoxyl groups in the lignin. Above 400 °C, methane is an

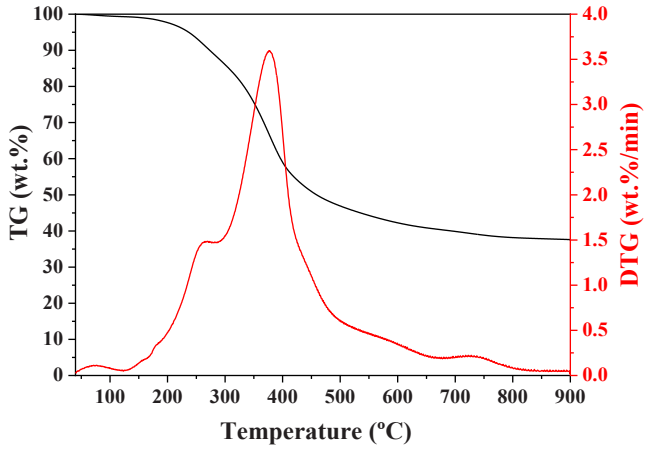

Fig. 1. TG and DTG curves obtained under nitrogen atmosphere of the lignin employed as feedstock.

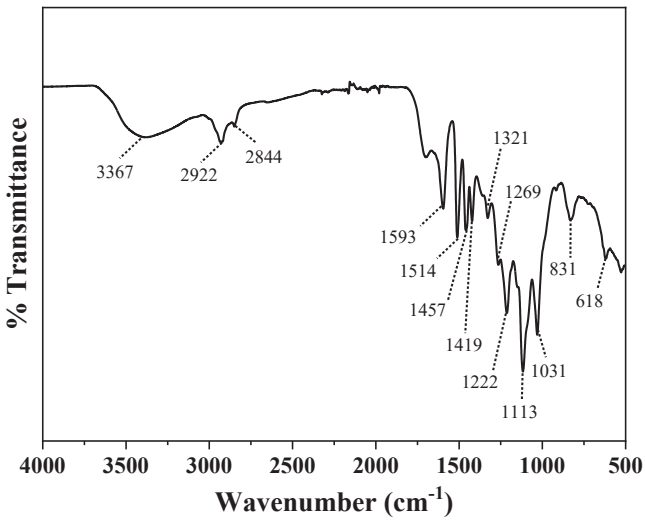

Fig. 2. ATR-FTIR spectrum of the lignin employed as feedstock.

important product of lignin degradation originating from the cracking of the methoxy groups, whereas CO_2 and CO are also formed due to the cleavage of C-O-C and C═O bonds [27,33].

The main functional groups present in the lignin here employed as feedstock have been identified by ATR-FTIR analysis (Fig. 2). The broad band at 3367 cm^{-1} is related to the -OH stretching vibration of aliphatic and phenolic hydroxyl groups. The signals at 2922 and 2844 cm^{-1} are attributed to C-H stretching of aliphatic structure, i.e. CH_2 and CH_3 groups. The bands at 1593 and 1514 cm^{-1} are derived from C-C stretching of aromatic rings. Furthermore, the 1321 and 1269 cm^{-1} peaks are assigned to the C-O stretching and C-H aromatic of syringyl and guaiacyl moieties, respectively. The vibrational band at 1222 cm^{-1} is linked with symmetrical and asymmetrical extending of C-O connected to C═O group. Finally, the peaks from C-H stretching of residual polysaccharides of lignin can be observed at 1113 and 1031 cm^{-1}, and also in the last small signals detected (831 and 618 cm^{-1}) [5,27,34,35].

3.2. Catalysts characterisation

In the present work, two different commercial zeolites in their acid form, H-ZSM-5 (MFI; Si/Al = 52) and H-Beta (BEA; Si/Al = 20), have been partially ion-exchanged with alkali and alkaline-earth metal cations (Na^+, K^+ and Mg^{2+}) following the procedure explained in the experimental section. The main aim is to modify the acid/base

Table 2
Physicochemical and textural properties of commercial and ion-exchanged H-ZSM-5 and H-Beta zeolites.

Sample	m_{Me}[a] (wt. %)	Me/Al[b]	Si/Al[b]	S_{BET}[c] (m^2/g)	S_{MIC}[d] (m^2/g)	V_{MIC}[d] (cm^3/g)	V_{TOT}[e] (cm^3/g)
H-ZSM-5	**-**	**-**	**52**	**431**	**334**	**0.123**	**0.346**
MgH-ZSM-5	0.28	0.36	53	398	300	0.107	0.354
KH-ZSM-5	1.00	0.84	55	407	331	0.116	0.340
NaH-ZSM-5	0.89	1.28	54	413	321	0.115	0.350
H-Beta	**-**	**-**	**20**	**689**	**479**	**0.174**	**0.356**
MgH-Beta	0.37	0.22	23	692	463	0.168	0.369
KH-Beta	1.39	0.53	24	658	453	0.165	0.345
NaH-Beta	1.46	0.95	24	639	441	0.160	0.336

[a] Metal weight percentage (ICP-AES)
[b] Molar ratio (ICP-AES)
[c] BET surface area
[d] Micropore surface area and micropore volume (t-plot method)
[e] Total pore volume ($P/P_0 \approx 0.95$)

properties of the parent acid zeolites by substituting protons (H^+) with the aforementioned cations. Table 2 summarises both the mass percentage (m_{Me}; wt.%) and metal to aluminium molar ratio (Me/Al), determined by ICP-AES analyses, of the different catalysts. H-ZSM-5 and H-Beta zeolites show a more efficient cation exchange with alkali metals than when the alkaline-earth metal is employed ($Na^+ > K^+ > Mg^{2+}$). Regarding the H-ZSM-5 zeolite, the proportion of K^+ partially replacing H^+ protons (K/Al = 0.84) is more than twice the value of Mg^{2+} incorporated in the same zeolite (Mg/Al = 0.36), while Na^+ is ion-exchanged in the highest proportion (Na/Al = 1.28). As the maximum theoretical value (Me/Al) that could be attained if cationic species counterbalanced all the negative charges associated with Al atoms in the zeolite framework is 1 for K^+ and Na^+ cations and 0.5 for Mg^{2+}, the latter result implies that the NaH-ZSM-5 is over-exchanged by Na^+ cation. Excess Na^+ cations are probably in the form of surface sodium oxides (Na_xO_y), as it is later discussed [17,36–38]. A similar trend is observed over the H-Beta zeolite, with the Me/Al molar ratios equal to 0.22, 0.53 and 0.95, for the ion-exchanged cations, Mg^{2+}, K^+ and Na^+, respectively. Regarding the alkali metals, the more efficient ion exchange of Na^+ could be ascribed to its smaller ionic radius and higher electronegativity compared with K^+ [16,39]. On the other hand, Mg^{2+}, although having the smallest ionic radius and highest electronegativity of the cations tested, possesses the largest hydrated radius [17]. Moreover, Mg^{2+} cations must counterbalance two negative charges associated with two Al atoms, which additionally should be closely located. Consequently, magnesium exchange is less favoured than alkali metals exchange, leading to lower cation loadings in respect of its theoretical maximum Mg/Al molar ratio (0.5).

As it can be observed, although the mass amount (m_{Me}, wt.%) of metal cations incorporated in the zeolite structures is higher for H-Beta, attending to the Me/Al molar ratios, the ion exchange process is slightly more effective over the H-ZSM-5 zeolite. These differences can be related to the very different physicochemical and textural properties of both zeolites. As H-ZSM-5 zeolite possesses a lower aluminium content (Si/Al = 52) than H-Beta (Si/Al = 20), it would be expected a higher content of exchange cations over the latter, as occurs attending to the mass percentage of exchanged metals, but this is not enough to reach similar Me/Al molar ratios as those of the H-ZSM-5 zeolites. As discussed later, H-ZSM-5 displays a highly ordered MFI framework structure, where an elevated proportion of Al atoms generates available and effective ion exchange sites. On the contrary, H-Beta consists of an intergrowth of different polymorphs, which generates a framework structure (BEA) with crystallographic faults and defects. Consequently, the H-Beta-based samples display a poorer correlation between the amount of framework Al atoms and the proportion of effective ion-exchange sites than the H-ZSM-5-based zeolites.

TEM micrographs reveal that the parent H-ZSM-5 (Fig. S1) is a nanocrystalline zeolite with a relatively narrow crystal size distribution (30–80 nm), while the commercial H-Beta zeolite (Fig. S2) consists of particles with sizes around 100–400 nm where it is easy to appreciate its characteristic highly faulted intergrowth structure due to the random stacking of different polymorphs during its hydrothermal crystallisation [40]. Hence, as depicted in Table 3, the H-ZSM-5 zeolite possesses mostly Brønsted acid sites (L/B = 0.2), while the H-Beta exhibits an elevated proportion of Lewis acid sites (L/B = 1.3). Consequently, since ion-exchange proceeds preferentially over Brønsted acid centres, the H-Beta-based samples display a poorer correlation between the amount of Al atoms and the proportion of effective ion-exchange sites than the H-ZSM-5-based zeolites.

All the ion-exchanged catalysts suffer a partial substitution of H^+ by the corresponding metal cation, except for the sodium ion-exchanged H-ZSM-5, whose Na/Al molar ratio is almost 30% higher than its theoretical maximum. This excess of Na could be located on the H-ZSM-5 surface [17,37,38] as sodium oxide (Na_xO_y) clusters or could anchor to silanol defects (weak acid sites) through covalent linkages (Si-O-Na) [36]. However, no significant differences are observed in the XRD pattern of sodium exchanged H-ZSM-5 when compared to the commercial H-ZSM-5 zeolite (Fig. 3.a). Both samples exhibit the characteristic MFI framework diffraction peaks, and no other impurity related to Na_xO_y phase is detected in the NaH-ZSM-5 zeolite. The most plausible explanation for the location and form of the excess cations within the zeolite is in the form of surface sodium oxides (Na_xO_y) and probably this phase has not been detected due to the homogeneous and high dispersion of these oxides over the zeolite surface. However, attending to the CO_2-TPD analyses (Table 3), the NaH-ZSM-5 sample shows the highest maximum desorption temperature (T_{max} = 246 °C) in comparison to all the other catalysts (< 171 °C), which indicates the existence of stronger basic sites, probably due to the presence of sodium oxide on the surface of this zeolite [36].

Similarly, both potassium and magnesium exchanged H-ZSM-5 samples show the characteristic diffraction pattern of MFI framework-type zeolites and no impurity phases are detected, indicating that the metal ion exchange process does not significantly modify the crystallinity of the samples. Moreover, no important differences are detected between the XRD patterns of the parent H-Beta and the metal ion-exchanged H-Beta samples (Fig. 3.b), and only a certain decrease in the diffraction peak intensity at 23.5º is distinguished. In addition, no visible metal oxide particles are detected in the TEM micrographs (Figs. S1 and S2) of the ion-exchanged zeolites, while TEM-EDX elemental mapping (Figs. S3 and S4) demonstrates the homogeneous distribution of Na, K and Mg over both H-ZSM-5 and H-Beta particles.

Ar sorption experiments were performed to determine the effect of the cation loading in the textural properties of the ion-exchanged zeolites. Fig. 4 displays the Ar adsorption-desorption isotherms of the parent and metal-exchanged H-ZSM-5 and H-Beta zeolites. H-ZSM-5-based materials show the characteristic isotherm of nanocrystalline zeolites, exhibiting a notable Ar uptake at high relative pressures ($P/P_0 > 0.8$), which denotes the great importance of the intercrystalline macroporosity existing in this type of catalysts formed by small nanocrystals with a relatively narrow crystal size distribution (30–80 nm), as depicted in Fig. S1. In the case of the H-Beta-based zeolites, there is a remarkable adsorption at intermediate relative pressures ($0.1 < P/P_0 < 0.8$), consistent with the continuous and maintained Ar adsorption in the stacking defaults existing in this zeolite. The most remarkable fact is that, independently of the metal exchanged and the zeolite tested, ion-exchanged zeolites possess isotherms with almost identical shape and sorption performance to their corresponding parent zeolites, denoting that there are no drastic modifications in the porous properties after the ion exchange.

Table 2 summarises the textural properties of the different materials. The most noticeable result is the slight lowering in the surface area and volume of micropores for the ion exchanged zeolites compared with the H^+ form ones. This decrease is clearly linked to the lessening in the micropore filling with Ar of the ion-exchanged zeolites, which is consistent with the substitution of zeolite framework H^+ protons by

Table 3
Acid/base properties of HZSM-5 and H-Beta-based catalysts.

Sample	FTIR/PYR (150 °C)			CO_2-TPD	
	BAS[a] (mmol/g)	LAS[b] (mmol/g)	L/B[c]	mmol/g	$T_{B\text{-}max}$ (°C)
H-ZSM-5	**0.215**	**0.049**	**0.2**	**0.009**	**173**
MgH-ZSM-5	0.116	0.165	1.4	0.022	124
KH-ZSM-5	0.006	0.175	29	0.017	171
NaH-ZSM-5	0.018	0.253	14	0.012	246
H-Beta	**0.205**	**0.266**	**1.3**	**0.003**	**118**
MgH-Beta	0.163	0.376	2.3	0.003	160
KH-Beta	0.065	0.326	5.0	0.003	104
NaH-Beta	0.006	0.411	68	0.002	102

[a] Concentration of Brønsted Acid Sites
[b] Concentration of Lewis Acid Sites
[c] LAS/BAS molar ratio

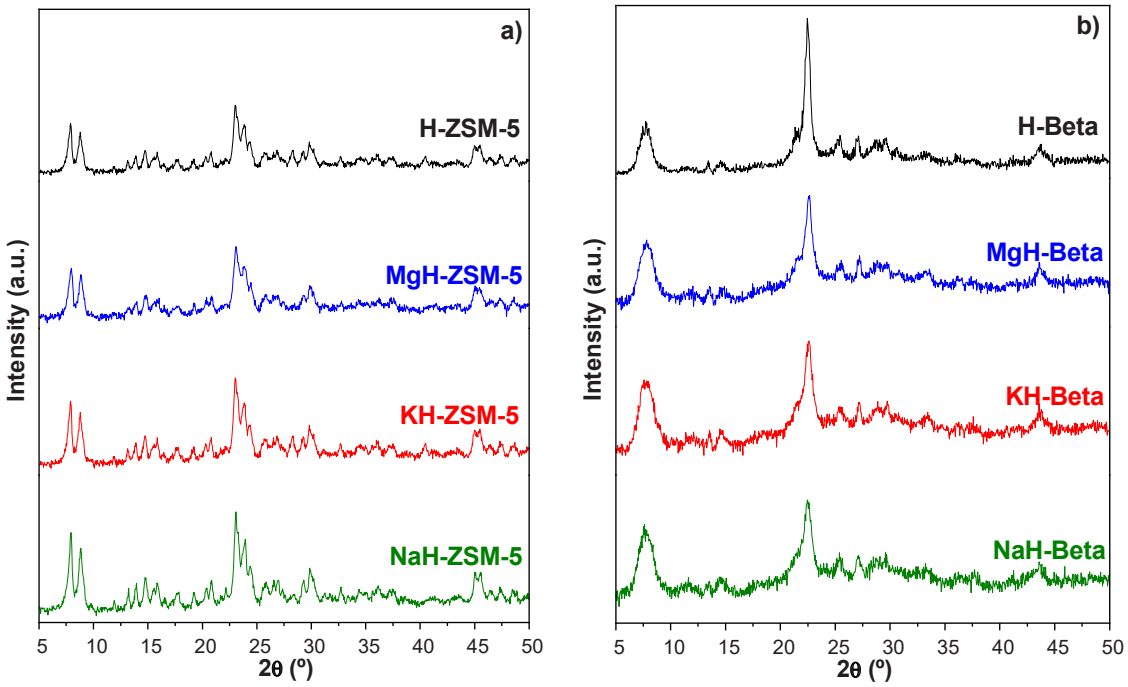

Fig. 3. XRD patterns of commercial and ion-exchanged a) H-ZSM-5, and b) H-Beta zeolites.

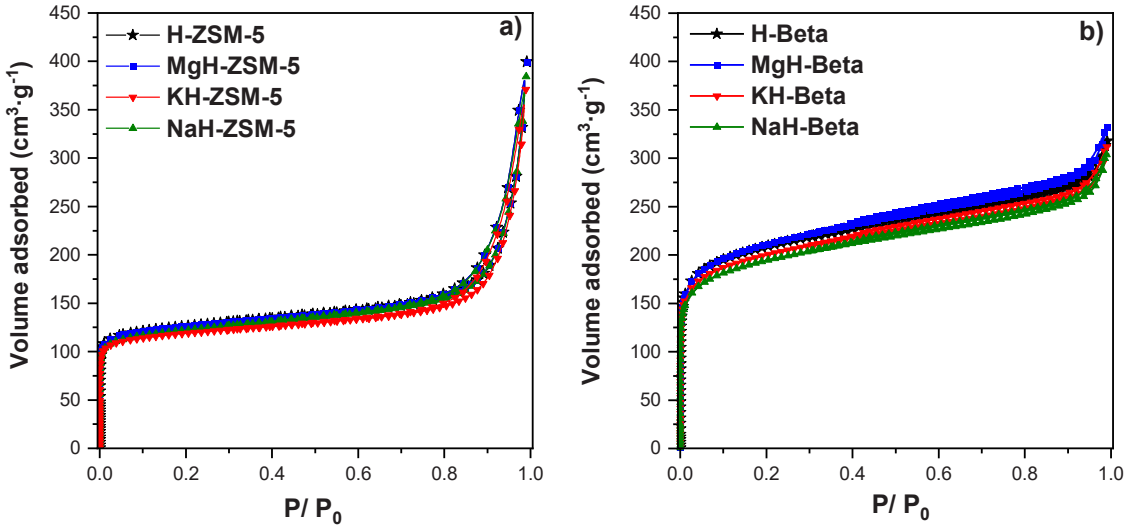

Fig. 4. Argon adsorption-desorption isotherms of commercial and ion-exchanged: a) H-ZSM-5, and b) H-Beta zeolites.

cations with larger ionic radius and, therefore, with the reduction in the values of the micropore volume (V_{MIC}) and micropore surface area (S_{MIC}).

Table 3 provides the main acid/base properties of the different catalysts. FTIR analyses of adsorbed pyridine at different temperatures provided a deep insight into identifying and quantifying the type, nature, and strength of the acid centres existing in the different samples. The commercial H-ZSM-5 zeolite is conformed mainly by Brønsted acid sites, BAS (L/B molar ratio = 0.2), of relatively high strength. As can be seen in Fig. 5.a, almost 50% of this type of acid centre is retained even when the FTIR spectrum is recorded after pyridine desorption at 450 °C. Magnesium exchange of the H-ZSM-5 zeolite reduces by almost 50% the concentration of Brønsted acid centres and increases more than three times the content of Lewis acid sites (LAS). Attending to Fig. 5.a and 5.b, both types of acid sites, BAS and LAS, could be classified as strong Brønsted-type and medium-strength Lewis-type acid centres, respectively. Similarly, KH-ZSM-5 is mainly composed of very weak LAS (L/B = 29), while NaH-ZSM-5 consists essentially of weak LAS, confirming the high degree of ion-exchange achieved with this cation. These results agree well with those attained by other authors [41], who determined that alkali-exchanged ZSM-5 zeolite possessed mainly weak acid strength (Lewis-type sites), decreasing the acid strength as the atomic weight of the exchanged cation increased.

CO_2-TPD measurements were performed aiming to evaluate the basicity of the H-ZSM-5-based materials (Table 3). Metal exchange hardly increases the amount of CO_2 adsorbed on the zeolite, the highest changes being denoted over the magnesium and potassium-exchanged zeolites, showing weak CO_2 adsorption that can be mainly attributed to molecularly adsorbed CO_2 [37]. These results agree with previous works [15,18], where it is established that alkali-exchanged ZSM-5

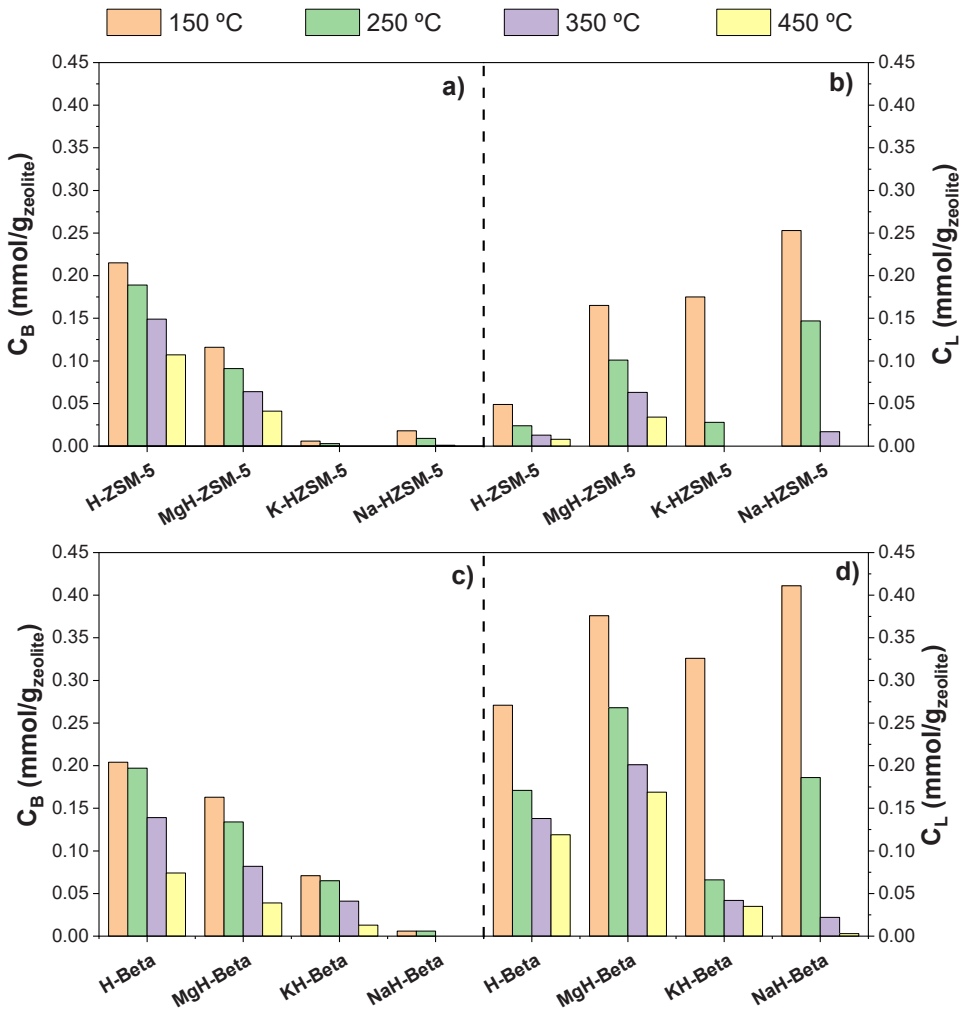

Fig. 5. Concentration of a,c) Brønsted (C_B), and b,d) Lewis (C_L) acid sites of the zeolites, probed by FTIR/pyridine adsorption, as a function of the outgassing temperature.

zeolites exhibit mainly weak basic centres. Higher CO_2 adsorption could be expected for the Beta zeolite family materials due to their higher Si/Al molar ratio and metal content, in comparison to ZSM-5 zeolites. However, during CO_2-TPD analyses, after CO_2 saturation the samples were purged under He flow and weakly adsorbed CO_2 can desorb and diffuse more easily over the Beta framework than over the ZSM-5 one because Beta zeolite presents higher external surface area (and structural defects due to its polymorph character), being detected a lower amount of this molecule during the TPD experiment.

The acid properties of the commercial H-Beta zeolite are notably different to those of the parent H-ZSM-5 zeolite. The commercial H-Beta zeolite initially displays a well-balanced Lewis/Brønsted acidity (L/B= 1.3), which is consistent with its elevated aluminium content (Si/Al = 20) and the singular distorted and faulted framework structure of this zeolite and, similarly to H-ZSM-5, after ion-exchange its acid nature turns mostly into Lewis-type (Fig. 5.c and 5.d). Accordingly, L/B molar ratios of 2.3, 5.0 and 68 are quantified over MgH-Beta, KH-Beta, and NaH-Beta, respectively. For these H-Beta-based catalysts, the acid strength (BAS and LAS) follows the same order: H-Beta > MgH-Beta > KH-Beta > NaH-Beta. These results correlate well with the grade of cation-exchange attained over the different materials. As the cation loading enhances, the L/B molar ratio increases, and the acid strength diminishes. Finally, regarding the basicity of these zeolites (Table 3), no significant concentration of strong basic sites is measured over any ion-exchanged Beta zeolite.

3.3. Catalytic fast pyrolysis of lignin employing MeH-ZSM-5 and MeH-Beta zeolites

In this section, the effect of the ion exchange with three metals, concretely, magnesium, potassium, and sodium, and two nanocrystalline zeolites, H-ZSM-5 and H-Beta, has been investigated in the catalytic fast pyrolysis of pure lignin. Based on previous studies published by the research team on the catalytic pyrolysis of lignocellulosic biomass [18, 19], and taking into account the lignin temperature decomposition observed in thermogravimetric analysis (see Fig. 1), temperatures of 550 and 450 °C were selected for the thermal and catalytic zones, respectively. Similarly, the amount of lignin fed into the process was 4 g, and catalyst-to-lignin (C/L) ratios of 0.2 and 0.4 were employed to evaluate the effect of the catalyst on products distribution. Finally, a non-catalytic test was also carried out, under the same reaction conditions, for comparison purposes.

The yield of the main fractions obtained in the lignin pyrolysis tests are summarised in Fig. 6.a and 7.a. Firstly, it is important to highlight that since the thermal pyrolysis step is common in all the reactions, the amount of char accumulated in the first reactor bed was quite similar, showing values around 40 wt.%. Therefore, it can be confirmed that the catalyst incorporation does not influence the char yield since thermal and catalytic zones are fully independent. In addition, the relevance in yield terms of char production is verified because this fraction accounts for 36% of the chemical energy contained in the initial lignin. Then, to achieve a sustainable process of lignin valorisation, the char could be

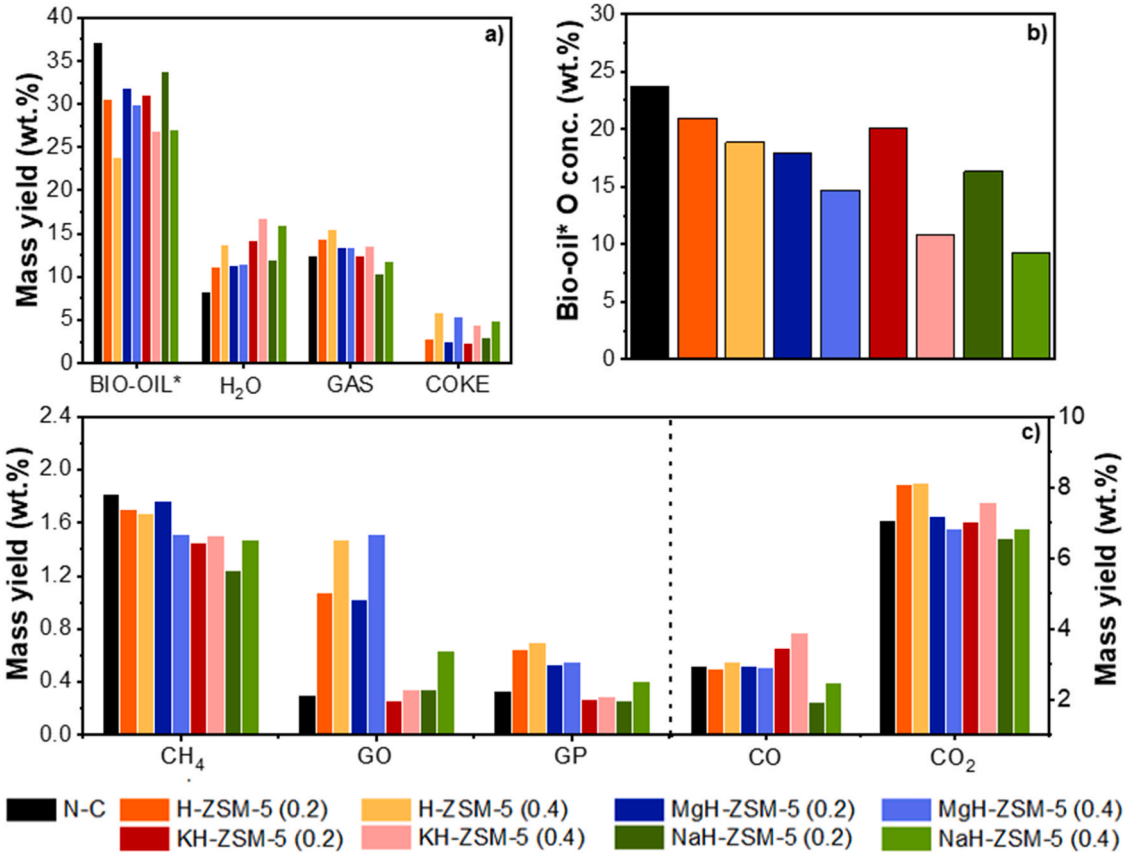

Fig. 6. Catalytic pyrolysis of lignin over commercial and ion-exchanged H-ZSM-5 zeolites: a) fractions yield; b) bio-oil* oxygen concentration (dry basis); c) gaseous components yield (GO: gaseous olefins, GP: gaseous paraffins).

burnt to provide the energy consumed in the own pyrolysis, achieving an energy-self-sufficient process [42]. Other uses of this residue have been investigated, such as to produce syn-gas or hydrogen [43].

In the case of catalytic experiments, coke is deposited over the catalyst surface promoted by repolymerisation and condensation reactions of the derived-lignin phenolics [44]. Finally, bio-oil and non-condensable gases are products of thermal and catalytic tests, being the first one accounted for on a water-free basis (bio-oil*).

Regarding the pyrolysis products distribution (Fig. 6.a and 7.a) it can be observed that the use of H-ZSM-5 and H-Beta commercial zeolites, and also the increment of the C/L ratio, give rise to a decrease in the bio-oil* yields due to the enhanced production of water, gases and coke, which can be related to the vapours from the thermal zone reacting subsequently over the catalyst bed. Several studies reported that the lignin decomposition pathway seems closely related to the concentration, type and strength of catalyst acid/basic sites and the textural properties of the catalyst employed [12,37,44–48]. The H-ZSM-5 zeolite sample presents a lower total acidity than H-Beta zeolite, according to its higher Si/Al ratio (Si/Al = 52) and FTIR/PYR analyses. However, its Brønsted acid sites exhibit slightly greater strength and higher concentration. Moreover, the total concentration of acid sites (LAS and BAS) is larger in H-Beta zeolite, but the more relevant difference is in the molar ratio L/B of both zeolites, being 0.2 and 1.3 for H-ZSM-5 and H-Beta, respectively. Thus, although both zeolites exhibit almost similar bio--oil* yields, H-Beta zeolite enhances water production, doubles the coke production and reaches a bio-oil* with the lowest oxygen concentration. Since bio-oil* upgrading is linked with the reduction of its oxygen content, in CFP, the deoxygenation can occur via three pathways: decarbonylation, decarboxylation and dehydration, releasing CO, CO_2 and H_2O, respectively [49]. Compared with the non-catalytic test, the water and non-condensable gas yields obtained in the CFP of lignin over H-Beta and H-ZSM-5 zeolites show that dehydration is the predominant route for both catalysts, but it is more favoured using the former. In addition, it is enhanced with a larger C/L ratio, which agrees with the decrease of the oxygen content of bio-oil* (Fig. 6.b and 7.b for HZM-5 and H-Beta zeolites, respectively).

CH_4, CO and CO_2 are the main components of the condensable gases, as can be observed in Fig. 6.c and 7.c. Hydrogen yields were almost negligible for all the tests (around 0.01 wt.%). Concerning CO and CO_2, the decarbonylation pathway is practically the same as for the thermal test, and the decarboxylation route is increased to a greater extent for both parent catalysts, being higher in the case of H-ZSM-5. Besides that, the presence of a catalyst implies cracking reactions that lead to the formation of gaseous hydrocarbons, i.e., methane and both light olefins (GO) and paraffins (GP), which are also represented in Fig. 6.c and 7.c for both parent zeolites. The yield of GO and GP are enhanced due to cracking and dealkylation reactions. In particular, ethylene and propylene serve as precursors to produce aromatics in the channels of the zeolites. The highest yield observed in H-ZSM-5 can be related to its slightly stronger BAS and almost the absence of LAS [12,44,50].

On the other hand, the coke fraction is generated by a complex combination of reactions, such as olefin oligomerisation and aromatics polycondensation, which are mainly catalysed by BAS [12]. The size and volume of micropores are another important factor determining the formation of carbonaceous residues in zeolites. Thus, larger micropores and higher micropore volumes involve higher coke yields [47]. This by-product is deposited over the catalysts, blocking the access to active sites and reducing the catalyst activity [51]. H-Beta zeolite exhibited a higher coke yield than H-ZSM-5, increasing according to C/L ratio with values of 2.6 wt.% (C/L = 0.2) and 5.9 wt.% (C/L = 0.4) for H-ZSM-5 and 5.6 wt.% (C/L = 0.2) and 10.8 wt.% (C/L = 0.4) for H-Beta. This behaviour agrees well with the higher micropore size and volume of

H-Beta zeolite. In addition, the coke elemental composition can help to understand the lowest oxygen content of bio-oil* obtained using H-Beta as catalyst compared with H-ZSM-5 (Fig. 6.b and 7.b, respectively). These analyses of coke fractions are summarised in Table S1 and S2, for H-ZSM-5 and H-Beta zeolites, respectively, and both evaluated C/L ratios. The coke produced in the CFP test over H-Beta presents more significant oxygen contents than those with H-ZSM-5 zeolite due to the accumulation of oxygenated species in this residue.

Significant changes are observed in the distribution of the products by fractions in the pyrolytic tests after the ion-exchanged of H-ZSM-5 and H-Beta with Na^{+}, K^{+} and Mg^{2+} (Fig. 6 and 7). These results indicate that the ion-exchanged zeolites present different behaviour for the conversion of the thermal vapours due to the altered distribution of LAS and BAS provoked by the metal incorporation [48]. In particular, H-ZSM-5 zeolite shows a high BAS concentration (0.215 mmol/$g_{zeolite}$) and a poor contribution of LAS resulting in a L/B ratio of 0.2. The incorporation of metals provokes an increase in the concentration of LAS with a significant reduction of the BAS proportion, reaching L/B ratios of 14 and 29 for NaH-ZSM-5 and KH-ZSM-5, respectively. These variations in the acid features of the zeolite cause an increase in bio-oil* yield, a decrease in permanent gas production and significant water production, which are especially remarkable for the C/L ratio of 0.4. NaH-ZSM-5 zeolite reaches lower oxygen concentration in bio-oil* due to dehydration reactions being promoted to a greater extent [23,48]. Between both zeolites, the most important changes related to the parent zeolite is for that ion-exchanged with sodium, which can be ascribed to the higher loading of this cation (Table 2) [12,52]. In the case of the magnesium-containing zeolite, the BAS and LAS are more balanced, with a L/B molar ratio of 1.4 and exhibit the highest concentration of basic centres (0.022 mmol CO_2/$g_{zeolite}$). Thus, the products yield distribution is quite similar to the parent zeolite, with a slightly better bio-oil* yield and a slight decrease in the bio-oil* oxygen content attributed to its basic features [15,18] and the presence of LAS due to the incorporation of metal.

In general, H-Beta based metal ion-exchanged catalysts show similar behaviour with respect to their H-ZSM-5 counterparts, producing lower oxygen concentration in the bio-oil* , and increasing the generation of water and coke, being these effects more pronounced for the higher value of the C/L ratio (0.4). As for MeH-ZSM-5 zeolites, dehydration reactions are highly promoted over MeH-Beta catalysts. Furthermore, coke production is also boosted over these zeolites, doubling the coke yield compared to MeH-ZSM-5 zeolites. These effects are especially relevant over the alkali-exchanged H-Beta zeolites. Thus, for the C/L ratio of 0.4, KH-Beta produces a bio-oil* with the lowest oxygen concentration (~7.2 wt.%), a value very close to that attained over the NaH-Beta (~7.8 wt.%). Similarly, the values of coke yield are also the highest when both zeolites are tested (~13 wt.% for NaH-Beta and KH-Beta zeolites). These zeolites contain mostly Lewis acid centres, exhibiting L/B molar ratios remarkably higher than those shown by both the parent acid and the magnesium-exchanged zeolites. MgH-Beta, exhibiting a Lewis acid density between that of the H-Beta and the alkali-exchanged H-Beta zeolites, also shows a product yield distribution between both types of zeolites. The oxygen concentration in the bio-oil* produced over this zeolite is close to that obtained when the H-Beta zeolite is employed, while the bio-oil* and the coke mass yields are close to those attained over the alkali-exchanged H-Beta zeolites.

The components present in the bio-oil* fraction have been determined employing GC-MS analyses, using calibration methods of the major products present in each family to get quantitative data regarding mass yield related to the raw lignin fed and concentration in the bio-oil* . Although the results are expressed in water free basis of liquid product, i.e. bio-oil* , aqueous and organic phases of the bio-oil were

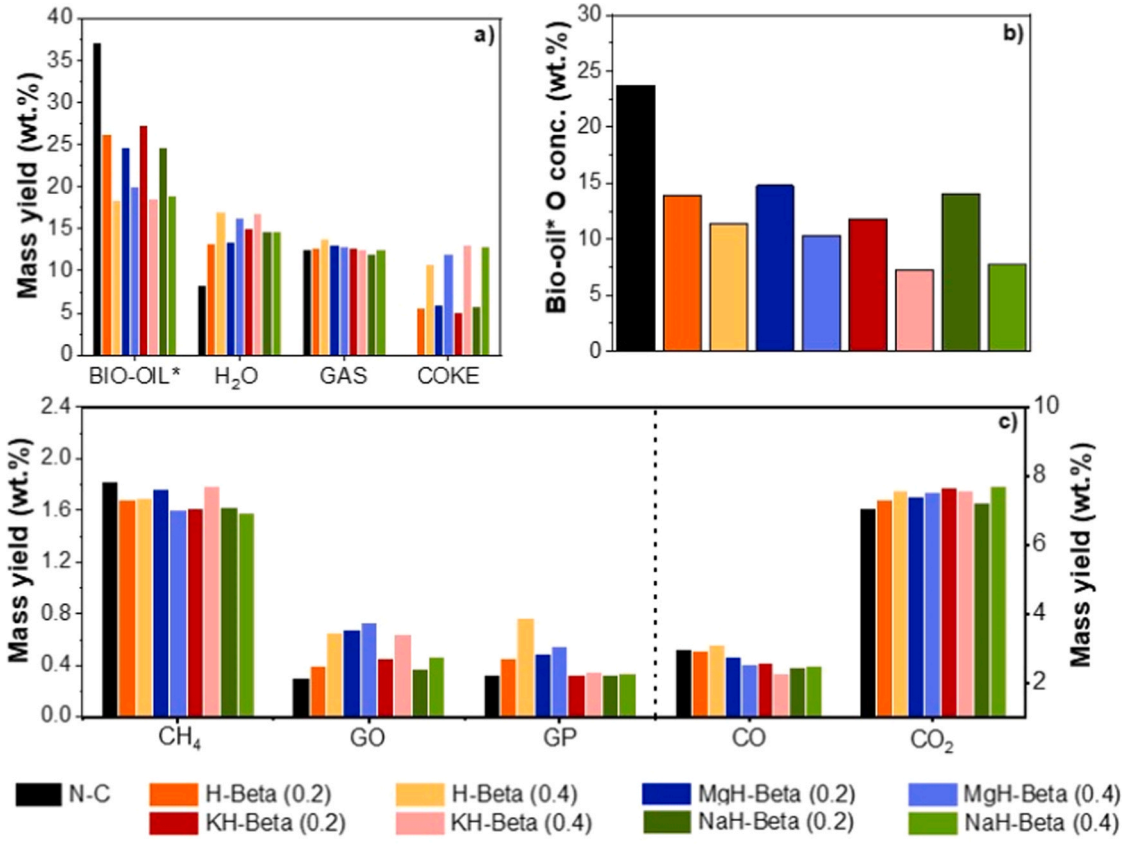

Fig. 7. Catalytic pyrolysis of lignin over commercial and ion-exchanged H-Beta zeolites: a) fractions yield; b) bio-oil* oxygen concentration (dry basis); c) gaseous components yield (GO: gaseous olefins, GP: gaseous paraffins).

separately analysed to determine the distribution of the different compound families in both phases, classified according to their chemical nature in the following five groups: carboxylic acids (CA), light oxygenates (LO, mainly ketones, aldehydes and esters), furans (FUR), aromatics (AR) and oxygenated aromatics (O-AR). Related to bio-oil* yield calculations, these were performed by subtracting the water content (quantified through Karl Fischer titration) from the total produced bio-oil (measured by weighing) and then normalising it to the amount of biomass initially fed into the system. Furthermore, the components in the bio-oil* were identified by GC-MS and, by difference, those not detected were determined, mainly including heavy/oligomeric species. These GC-MS results can be expressed as yield relative to the biomass fed into the pyrolysis process (Mass yield, wt.%) or as concentration in the obtained bio-oil* (Concentration, wt.%). The best catalyst will promote lignin decomposition, increasing the detected proportion of bio-oil*-compounds. As can be observed in Fig. 8.a and 9.a, the detected components in the bio-oil* obtained from the thermal pyrolysis are around 14 wt.%, and their concentration in the bio-oil* fraction is below 40 wt.% (Fig. 8.b and 9.b). Therefore, more than half of the bio-oil* is formed by oligomers and heavy species that cannot be detected by GC-MS, coming from the partial fragmentation of lignin or formed through cross-reactions between the bio-oil* components [53]. Fig. 8.a and 9.a summarise the mass yield of both GC-MS detected and non-detected compounds in bio-oil* for the parent H-ZSM-5 and H-Beta zeolites and the metal ion-exchanged ones. The use of H-ZSM-5 and H-Beta zeolites as catalysts achieves a significant increase in the detected compounds, being higher for the former due to the strength and concentration of its BAS. Brønsted acid centres promote cracking and dehydration reactions of thermal vapours to form small olefins that are transformed into aromatic hydrocarbons (AR). In addition, this type of acidity promotes dealkylation reactions to produce alkoxyphenols, which can be transformed into alkylphenols by dealkoxylation reactions [44]. Thus, H-ZSM-5 exhibit higher yields of aromatic hydrocarbons (AR), light oxygenates (LO) and oxygenated aromatics (O-AR) than H-Beta (Fig. 8.c and 9.c), whose acidity is more balanced with a similar concentration of BAS and LAS.

On the other hand, except for NaH-Beta zeolite, incorporating metal ion-exchanged H-Beta zeolites as catalysts in CFP of lignin leads to a relevant increase in the concentration of GC-MS detected compounds, being higher according to the increase of the C/L ratio, which can be ascribed to the LAS promoting lignin decomposition reactions. Therefore, these catalysts are able to transform oligomers and heavy species into compounds with molecular size/boiling points within the bio-oil* detected fraction [19]. However, this trend does not apply for the NaH-Beta zeolite, which exhibits almost similar GC-MS detected compounds as the thermal reaction. It can be attributed to the largest amount of metal ion-exchange of all the zeolites studied (1.46 wt.%), and this high loading could promote condensation and polymerisation reactions, which is agree with the lower bio-oil* oxygen concentration obtained with this zeolite and, consequently, the cracking of heavy/oligomeric species to GC-MS detected ones are counteracted. It can also be observed that the ion-exchanged zeolites that remain significant Brønsted acidity, in particular, MgH-ZSM-5, MgH-Beta and KH-Beta, exhibit significant yield to aromatic hydrocarbons (AR), similar or even higher in the case of the MgH-Beta zeolite due to presents a concentration of BAS similar to the parent zeolite (0.163 mmol/g and 0.205 mmol/g, respectively).

Fig. 8.c and 9.c illustrate the products distribution per family in the bio-oil* fraction. Concretely, bio-oil* from the non-catalytic test contains mainly oxygenated aromatic compounds with a concentration of 33 wt.%, which are produced since the C-C and C-O bond cleavage of the dimers and larger alkoxyphenols formed from the depolymerisation of the lignin structural units: hydroxyphenyl, syringyl and guaiacyl [5,6]. Other families in this thermal bio-oil* (CA, LO, FUR and AR) do not

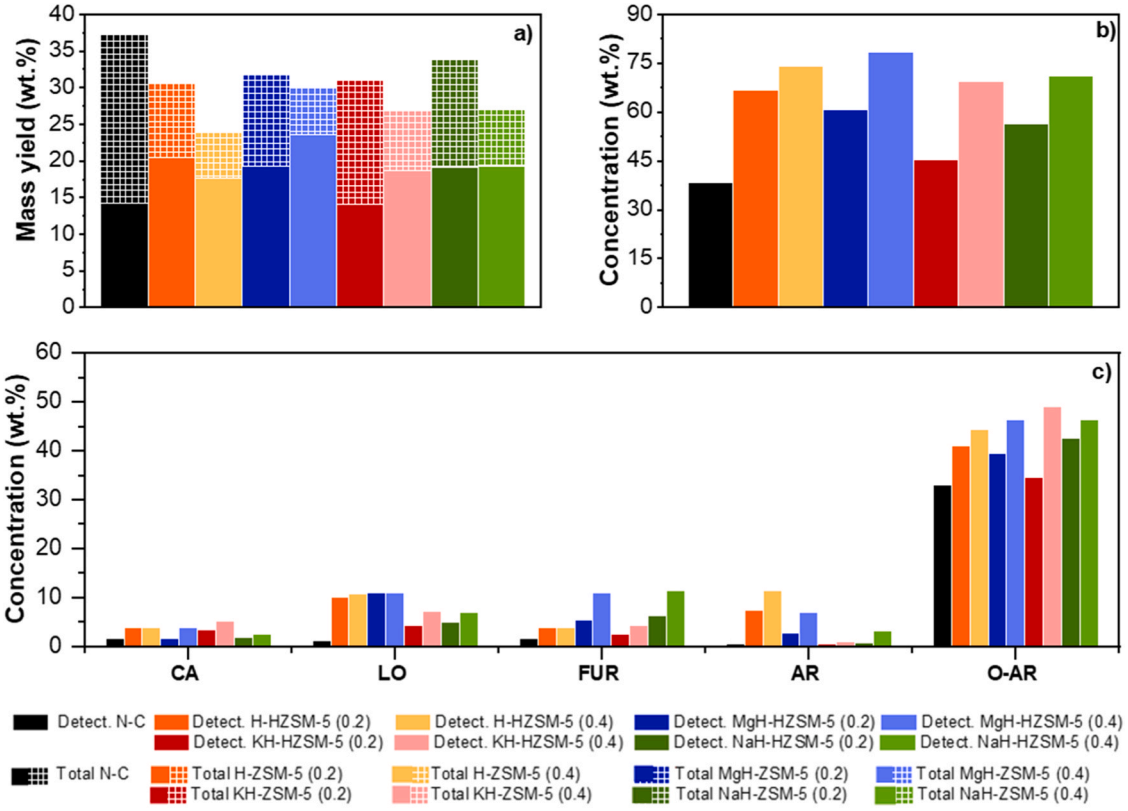

Fig. 8. GC-MS analyses of the bio-oil* obtained in the lignin catalytic pyrolysis over commercial and ion-exchanged H-ZSM-5 zeolites: a) overall mass yields; b) overall concentration of GC-MS detected components; and c) mass yields of compound families (CA: carboxylic acids, LO: light oxygenates, FUR: furans, AR: aromatic hydrocarbons and A-OR: oxygenated aromatics).

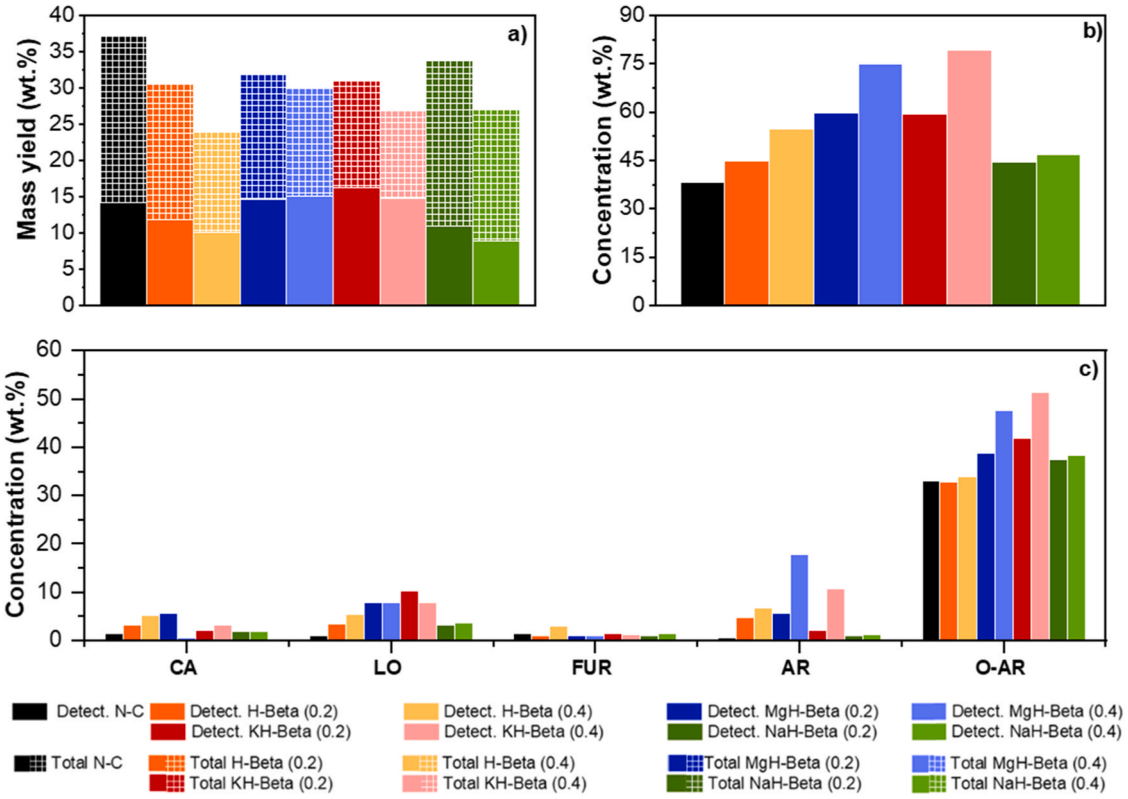

Fig. 9. GC-MS analyses of the bio-oil* obtained in the lignin catalytic pyrolysis over commercial and ion-exchanged H-Beta zeolites: a) overall mass yields; b) overall concentration of GC-MS detected components; and c) mass yields of compound families (CA: carboxylic acids, LO: light oxygenates, FUR: furans, AR: aromatic hydrocarbons and A-OR: oxygenated aromatics).

exceed 4.5 wt.%, being the lowest the aromatic hydrocarbons with a yield below 0.5 wt.%. In contrast, very different results arise from using H-ZSM-5 and H-Beta zeolites as catalysts. Lignin decomposition over these acid zeolites involves the production of CA, LO, FUR, AR and O-AR. In the case of aromatic hydrocarbons, the yield increase can be related to the fact that phenolic compounds are adsorbed on the acid sites forming multi-phenyl species via condensation. Then, the AR are produced from the cracking of these phenyl species. In addition, acid zeolites promote cracking reactions of lignin dimers or side chains to produce olefines that, via aromatisation, produce aromatic hydrocarbons (AR) [44,47,54,55]. H-ZSM-5 exhibits a higher yield of oxygenated aromatics than H-Beta, whose yield is quite similar to the thermal test. This finding shows that the H-ZSM-5 catalysts promote the conversion of lignin oligomers into oxygenated aromatics through cracking, dealkylation and dehydration reactions [54].

Fig. 10.a and 10.b summarise the concentration in the bio-oil*-fraction of the main components included in the oxygenated aromatics family. Regarding the non-catalytic lignin pyrolysis, it can be observed that the detected compounds are mainly alkylphenols (4.1 wt.%), syringols (9.32 wt.%) and guaiacols (18.1 wt.%). Taking into account that the phenolic-derived compounds of the lignin can be three types (hydroxyphenyl, syringyl and guaiacyl), it can be expected that the thermal degradation at 550 °C promotes the depolymerisation of lignin firstly, whereas the larger alkoxyphenols so-produced are transformed into small ones through cleavage of C-C and C-O bonds. The demethoxylation of these oxygenated products to alkylphenols is not favoured under thermal conditions [12]. Once acid zeolites are incorporated into the catalytic bed zone, relevant changes can be denoted. Demethoxylation reactions (C-O cleavage) are enhanced, as can be verified with the increase of alkylphenol concentration until 12.4 wt.% and 9.73 wt.% for H-ZSM-5 and H-Beta, respectively for the higher C/L ratio, and the reduction of guaiacols concentration (14.6 and 13.86 wt.% for H-ZSM-5 and H-Beta, respectively, for C/L ratio of 0.4). However, syringols family proportion in bio-oil* increases just for H-ZSM-5 (12.75 wt.% for C/L = 0.4), which can be related to their stronger BAS promoting cracking and dealkylation of the larger alkoxyphenols produced in the thermal zone [44]. Another important difference is the presence of a more significant amount of methoxybenzenes (MTB) when both zeolites are employed in the process due to the methylation of phenolic compounds [56]. Regarding the O-AR concentration for ion-exchanged H-ZSM-5 and H-Beta zeolites, it can be appreciated that a relevant increase of guaiacols takes place for the Na^+ and K^+ zeolites, related to their higher L/B acid sites molar ratio, commented previously in FTIR/PYR analyses, concretely reaching values around 24 wt.% for the larger C/L ratio and MeH-ZSM-5. Significant differences are observed for the Mg^{2+} and K^+ catalysts. The alkylphenols production is notably higher for MgH-Beta and KH-Beta zeolite than in the corresponding MeH-ZSM-5 ones. This behaviour can be attributed to their more balanced concentration of LAS and BAS, which encourage demethoxylation reactions. The concentration of catechols and methoxybenzenes for all ion-exchanged zeolites is enhanced compared with the thermal experiment results, which are formed by demethoxylation of syringil groups and methylation reactions of alkylphenols [44,46].

Finally, Tables S3 and S4 detail the concentration in the bio-oil*-fraction of the main components included in the O-AR family. Among the produced O-AR, guaiacols, phenols and syringols subfamilies are predominant in all the pyrolysis tests. However, the use of metal catalysts with different acid properties implies a significant increase in water production, which hydrolyse the β-O-4 linkages, promoting the formation of products of these families [57]. Guaiacol, ethylguaiacol and creosol are the main components obtained in the guaiacol family. They can be used as starting materials for cosmetics formulation and pesticides and as platform molecules in the pharmaceutical industry [58]. Among large phenolics compounds obtained in CFP of lignin,

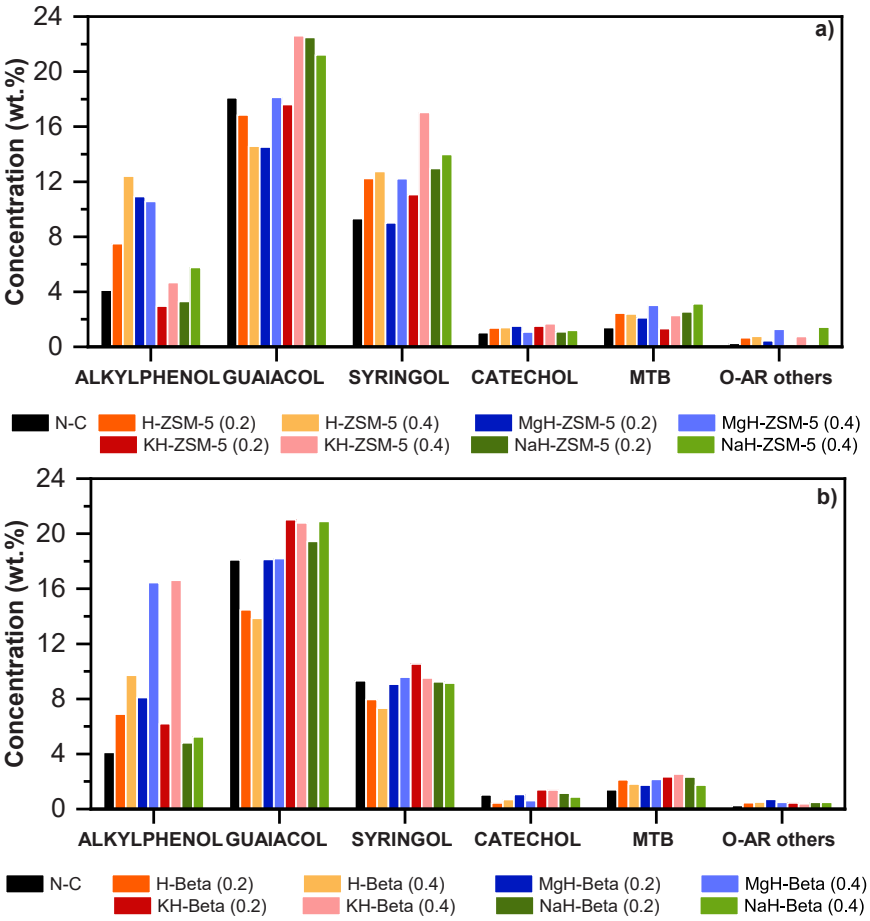

Fig. 10. Detail of aromatic oxygenated compounds obtained in the lignin catalytic pyrolysis over commercial and ion-exchanged zeolites: a) H-ZSM-5, and b) H-Beta (MTB: methoxybenzenes).

methylphenol and dimethylphenol can be used as raw material in the polymer industry and for the synthesis of surfactants, fuel additives and resins [15]; and syringols are employed as flavours in the food industry [59].

In summary, the incorporation by ion-exchange of sodium, potassium and magnesium over H-ZSM-5 and H-Beta leads to materials that can be used as catalysts in the CFP of lignin to favour the increase of GC-MS detected compounds in the bio-oil* and the selectivity towards oxygenated aromatic products. The best behaviour was obtained using MgH-ZSM-5, MgH-Beta and KH-Beta materials due to the increase of detected fraction in bio-oil* . The results here explained to produce phenolic-derived compounds implies an important advance to the valorisation of this biomass-derived product to obtain high-value products that can be used as raw chemicals for fine chemistry applications and avoid this production from fossil fuels.

4. Conclusions

The catalytic fast pyrolysis of lignin Protobind 1000 has been investigated using two parent acid-form zeolites (H-ZSM-5 and H-Beta) and their homologous alkali (Na^+ and K^+) and alkaline-earth (Mg^{2+}) ion-exchanged forms. Although both parent zeolites possess very different physicochemical and textural properties, the ion-exchange effectiveness follows the same trend ($Na^+ > K^+ > Mg^{2+}$). No significant morphological or crystallographic changes are detected, and no metal oxide phases, or cation agglomeration has been distinguished. Cation exchange is predominantly produced over the Brønsted acid sites of both H-ZSM-5 and H-Beta parent zeolites, producing catalysts with an enhanced concentration of Lewis acid sites.

Compared to the non-catalytic fast pyrolysis of lignin Protobind 1000, it can be concluded that the catalytic process provokes a reduction of the bio-oil* yields while the production of water, gases, and coke increases. This is accompanied by a positive bio-oil* oxygen concentration lowering and a clear increase in the GC-MS detected compounds. Similarly, regarding the catalytic reactions, an increase in the catalyst to lignin mass ratio (C/L) has the same effect, suggesting the CFP water and non-condensable gas yields that dehydration is the main route for lignin deoxygenation in the catalytic process.

Both acid zeolites, H-ZSM-5 and H-Beta, lead to similar bio-oil*-yields. However, the H-Beta zeolite boosts the water production and generates a bio-oil* with the lowest oxygen concentration, whereas the coke produced is twice the amount generated over the H-ZSM-5 zeolite. These results are ascribed to the higher acidity and Lewis-type acid nature (L/B =1.3) of the H-Beta, in addition to the enhanced porosity and accessibility of this zeolite. However, the stronger Brønsted acid character of the H-ZSM-5 zeolite promotes cracking, dehydration, dealkylation and dealkoxylation reactions, giving rise to bio-oils* with a higher concentration of GC-MS detected components, and enhancing the production of light oxygenates, aromatics and oxygenated aromatic compounds.

The lowest bio-oil* oxygen concentration is attained when the cation-exchanged zeolites are tested, especially over KH-Beta and NaH-Beta zeolites, which is related to the promotion to a greater extent of dehydration reactions over these mainly Lewis-type acid zeolites. In addition, a proper balance between accessible Brønsted and Lewis acid sites (MgH-ZSM-5, MgH-Beta and KH-Beta) favours the production of a higher concentration of GC-MS detected compounds, mostly light oxygenates, and aromatics. On the other hand, the production of

oxygenated aromatics is improved by catalysts having enough proportion of accessible Brønsted and/or Lewis acid centres. Guaiacols and syringols are promoted to a greater extent by NaH-ZSM-5 and KH-ZSM-5 zeolites due to their elevated L/B molar ratios, while alkylphenols are mostly favoured over the MgH-Beta and KH-Beta zeolites owing to the existence of the proper combination of BAS and LAS (an adequate L/B molar ratio) in these materials if they are compared to the rest of the catalysts.

CRediT authorship contribution statement

M.I. Ávila: Investigation, Formal analysis, Data curation, Writing – original draft. **M.M. Alonso-Doncel:** Investigation, Formal Analysis, Writing – review & editing, **L. Briones:** Writing – review & editing, **G. Gómez-Pozuelo:** Conceptualization, Methodology, Data curation, Validation, Writing – original draft, Writing – review & editing. **J.M. Escola:** Conceptualization, Writing – original draft, Writing - review & editing, Funding acquisition. **D.P. Serrano:** Conceptualization, Methodology, Writing – review & editing, Funding acquisition, **A. Peral:** Conceptualization, Methodology, Formal analysis, Supervision, Validation, Writing – original draft, Writing – review & editing, **Juan Angel Botas:** Conceptualization, Methodology, Supervision, Validation, Writing – original draft, Writing – review & editing, Funding acquisition.

Declaration of Competing Interest

The authors declare that they have no known competing financial interests or personal relationships that could have appeared to influence the work reported in this paper.

Data Availability

No data was used for the research described in the article.

Acknowledgements

The authors gratefully acknowledge the financial support from the Science and Innovation Ministry and the Spanish Agency of Research through project ADBIOCAP (PID2020-114740RB-C22/AEI/10.13039/501100011033).

Appendix A. Supporting information

Supplementary data associated with this article can be found in the online version at doi:10.1016/j.cattod.2023.114419.

References

[1] C. Xu, M. Nasrollahzadeh, M. Selva, Z. Issaabadi, R. Luque, Waste-to-wealth: biowaste valorization into valuable bio(nano)materials, Chem. Soc. Rev. 48 (2019) 4791–4822, https://doi.org/10.1039/C8CS00543E.
[2] J. Zakzeski, P.C.A. Bruijnincx, A.L. Jongerius, B.M. Weckhuysen, The catalytic valorization of lignin for the production of renewable chemicals, Chem. Rev. 110 (2010) 3552–3599, https://doi.org/10.1021/CR900354U.
[3] K. Lopez Camas, A. Ullah, Depolymerization of lignin into high-value products, Biocatal. Agric. Biotechnol. 40 (2022), 102306, https://doi.org/10.1016/j.bcab.2022.102306.
[4] S. Constant, H.L.J. Wienk, A.E. Frissen, P. De Peinder, R. Boelens, D.S. Van Es, R.J. H. Grisel, B.M. Weckhuysen, W.J.J. Huijgen, R.J.A. Gosselink, P.C.A. Bruijnincx, New insights into the structure and composition of technical lignins: A comparative characterisation study, Green. Chem. 18 (2016) 2651–2665, https://doi.org/10.1039/c5gc03043a.
[5] H. Li, A.G. McDonald, Fractionation and characterization of industrial lignins, Ind. Crops Prod. 62 (2014) 67–76, https://doi.org/10.1016/j.indcrop.2014.08.013.
[6] X. Liu, F.P. Bouxin, J. Fan, V.L. Budarin, C. Hu, J.H. Clark, Recent Advances in the Catalytic Depolymerization of Lignin towards Phenolic Chemicals: A Review, ChemSusChem 13 (2020) 4296–4317, https://doi.org/10.1002/CSSC.202001213.
[7] F.P. Bouxin, A. McVeigh, F. Tran, N.J. Westwood, M.C. Jarvis, S.D. Jackson, Catalytic depolymerisation of isolated lignins to fine chemicals using a Pt/alumina catalyst: part 1—impact of the lignin structure, Green. Chem. 17 (2015) 1235–1242, https://doi.org/10.1039/C4GC01678E.
[8] X. Zhang, W. Jiang, H. Ma, S. Wu, Relationship between the formation of oligomers and monophenols and lignin structure during pyrolysis process, Fuel 276 (2020), 118048, https://doi.org/10.1016/J.FUEL.2020.118048.
[9] S.S. Wong, R. Shu, J. Zhang, H. Liu, N. Yan, Downstream processing of lignin derived feedstock into end products, Chem. Soc. Rev. 49 (2020) 5510–5560, https://doi.org/10.1039/D0CS00134A.
[10] G. Kabir, B.H. Hameed, Recent progress on catalytic pyrolysis of lignocellulosic biomass to high-grade bio-oil and bio-chemicals, Renew. Sustain. Energy Rev. 70 (2017) 945–967, https://doi.org/10.1016/J.RSER.2016.12.001.
[11] S. Wang, Z. Wan, Y. Han, Y. Jiao, Z. Li, P. Fu, N. Li, A. Zhang, W. Yi, A review on lignin waste valorization by catalytic pyrolysis: Catalyst, reaction system, and industrial symbiosis mode, J. Environ. Chem. Eng. 11 (2023), 109113, https://doi.org/10.1016/J.JECE.2022.109113.
[12] C. Wang, J. Ou, T. Zhang, S. Xia, S. Kang, S. Chen, A. Zheng, Z. Zhao, Sustainable aromatic production from catalytic pyrolysis of lignin mediated by a novel solid Lewis acid catalyst, Fuel 348 (2023), 128513, https://doi.org/10.1016/J.FUEL.2023.128513.
[13] A. Kumar, A. Kumar, J. Kumar, T. Bhaskar, Catalytic pyrolysis of soda lignin over zeolites using pyrolysis gas chromatography-mass spectrometry, Bioresour. Technol. 291 (2019), 121822, https://doi.org/10.1016/J.BIORTECH.2019.121822.
[14] V.B.F. Custodis, S.A. Karakoulia, K.S. Triantafyllidis, J.A. Van Bokhoven, Catalytic fast pyrolysis of lignin over high-surface-area mesoporous aluminosilicates: effect of porosity and acidity, ChemSusChem 9 (2016) 1134–1145, https://doi.org/10.1002/CSSC.201600105.
[15] C.A. Mullen, P.C. Tarves, A.A. Boateng, Role of potassium exchange in catalytic pyrolysis of biomass over ZSM-5: formation of alkyl phenols and furans, ACS Sustain. Chem. Eng. 5 (2017) 2154–2162, https://doi.org/10.1021/acssuschemeng.6b02262.
[16] S.T. Yang, J. Kim, W.S. Ahn, CO_2 adsorption over ion-exchanged zeolite beta with alkali and alkaline earth metal ions, Microporous Mesoporous Mater. 135 (2010) 90–94, https://doi.org/10.1016/j.micromeso.2010.06.015.
[17] R. Sharma, T. Segato, M.P. Delplancke, H. Terryn, G.V. Baron, J.F.M. Denayer, J. Cousin-Saint-Remi, Hydrogen chloride removal from hydrogen gas by adsorption on hydrated ion-exchanged zeolites, Chem. Eng. J. 381 (2020), 122512, https://doi.org/10.1016/J.CEJ.2019.122512.
[18] L.M. López-Renau, L. García-Pina, H. Hernando, G. Gómez-Pozuelo, J.A. Botas, D. P. Serrano, Enhanced bio-oil upgrading in biomass catalytic pyrolysis using KH-ZSM-5 zeolite with acid-base properties, Biomass-.-. Convers. Biorefinery 11 (2021) 2311–2323, https://doi.org/10.1007/s13399-019-00455-9.
[19] L.M. López-Renau, H. Hernando, G. Gómez-Pozuelo, J.A. Botas, D.P. Serrano, Utilisation of a basic K-grafted USY zeolite in catalytic pyrolysis of wheat straw to produce valuable oxygenated compounds, Catal. Today 390–391 (2022) 198–209, https://doi.org/10.1016/j.cattod.2021.11.034.
[20] V. Zholobenko, C. Freitas, M. Jendrlin, P. Bazin, A. Travert, F. Thibault-Starzyk, Probing the acid sites of zeolites with pyridine: Quantitative AGIR measurements of the molar absorption coefficients, J. Catal. 385 (2020) 52–60, https://doi.org/10.1016/J.JCAT.2020.03.003.
[21] B.M. Upton, A.M. Kasko, Strategies for the conversion of lignin to high-value polymeric materials: Review and perspective, Chem. Rev. 116 (2016) 2275–2306, https://doi.org/10.1021/acs.chemrev.5b00345.
[22] S.A. Channiwala, P.P. Parikh, A unified correlation for estimating HHV of solid, liquid and gaseous fuels, Fuel 81 (2002) 1051–1063, https://doi.org/10.1016/S0016-2361(01)00131-4.
[23] H. Hernando, S. Jiménez-Sánchez, J. Fermoso, P. Pizarro, J.M. Coronado, D. P. Serrano, Assessing biomass catalytic pyrolysis in terms of deoxygenation pathways and energy yields for the efficient production of advanced biofuels, Catal. Sci. Technol. 6 (2016) 2829–2843, https://doi.org/10.1039/c6cy00522e.
[24] S.V. Vassilev, D. Baxter, L.K. Andersen, C.G. Vassileva, An overview of the chemical composition of biomass, Fuel 89 (2010) 913–933, https://doi.org/10.1016/j.fuel.2009.10.022.
[25] Y. Bi, X. Lei, G. Xu, H. Chen, J. Hu, Catalytic Fast Pyrolysis of Kraft Lignin over Hierarchical HZSM-5 and Hβ Zeolites, 82, Catal 2018 Vol. 8 (8) (2018) 82, https://doi.org/10.3390/CATAL8020082.
[26] E. Leng, Y. Guo, J. Chen, S. Liu, J. E, Y. Xue, A comprehensive review on lignin pyrolysis: Mechanism, modeling and the effects of inherent metals in biomass, Fuel 309 (2022), 122102, https://doi.org/10.1016/j.fuel.2021.122102.
[27] S. Sahoo, M.Ö. Seydibeyoğlu, A.K. Mohanty, M. Misra, Characterization of industrial lignins for their utilization in future value added applications, Biomass-.-. Bioenergy 35 (2011) 4230–4237, https://doi.org/10.1016/j.biombioe.2011.07.009.
[28] E. Jakab, O. Faix, F. Till, Thermal decomposition of milled wood lignins studied by thermogravimetry/mass spectrometry, J. Anal. Appl. Pyrolysis 40–41 (1997) 171–186, https://doi.org/10.1016/S0165-2370(97)00046-6.
[29] N. Sallem-Idrissi, C. Vanderghem, T. Pacary, A. Richel, D.P. Debecker, J. Devaux, M. Sclavons, Lignin degradation and stability: Volatile Organic Compounds (VOCs) analysis throughout processing, Polym. Degrad. Stab. 130 (2016) 30–37, https://doi.org/10.1016/j.polymdegradstab.2016.05.028.
[30] T. Kotake, H. Kawamoto, S. Saka, Pyrolysis reactions of coniferyl alcohol as a model of the primary structure formed during lignin pyrolysis, J. Anal. Appl. Pyrolysis 104 (2013) 573–584, https://doi.org/10.1016/j.jaap.2013.05.011.
[31] M.J. Gan, Y.Q. Niu, X.J. Qu, C.H. Zhou, Lignin to value-added chemicals and advanced materials: extraction, degradation, and functionalization, Green. Chem. 24 (2022) 7705–7750, https://doi.org/10.1039/d2gc00092j.
[32] A. Tejado, C. Peña, J. Labidi, J.M. Echeverria, I. Mondragon, Physico-chemical characterization of lignins from different sources for use in phenol-formaldehyde

resin synthesis, Bioresour. Technol. 98 (2007) 1655–1663, https://doi.org/10.1016/j.biortech.2006.05.042.
[33] H. Yang, R. Yan, H. Chen, D.H. Lee, C. Zheng, Characteristics of hemicellulose, cellulose and lignin pyrolysis, Fuel 86 (2007) 1781–1788, https://doi.org/10.1016/j.fuel.2006.12.013.
[34] Nishu, Y. Li, R. Liu, Catalytic pyrolysis of lignin over ZSM-5, alkali, and metal modified ZSM-5 at different temperatures to produce hydrocarbons, J. Energy Inst. 101 (2022) 111–121, https://doi.org/10.1016/j.joei.2022.01.001.
[35] S. Vichaphund, P. Wimuktiwan, C. Soongprasit, V. Sricharoenchaikul, D. Atong, Aromatic and aliphatic production of catalytic pyrolysis of lignin using ZSM-5/Al-SBA-15 catalyst derived from high-calcium fly ash, Energy Rep. 7 (2021) 232–247, https://doi.org/10.1016/j.egyr.2021.07.127.
[36] J. Kim, J. Bang, J.-S. Choi, D. Lim, D. Gyeong Guk, J. Jae, Selective conversion of lactic acid to renewable acrylic acid over SDA-free Na-ZSM-5: The critical role of basic sites of sodium oxide, J. Catal. (2023), https://doi.org/10.1016/J.JCAT.2023.03.024.
[37] G. Busca, Acidity and basicity of zeolites: A fundamental approach, Microporous Mesoporous Mater. 254 (2017) 3–16, https://doi.org/10.1016/j.micromeso.2017.04.007.
[38] R.J. Davis, New perspectives on basic zeolites as catalysts and catalyst supports, J. Catal. 216 (2003) 396–405, https://doi.org/10.1016/S0021-9517(02)00034-9.
[39] K.S. Walton, M.B. Abney, M.D. LeVan, CO_2 adsorption in y and X zeolites modified by alkali metal cation exchange, Microporous Mesoporous Mater. 91 (2006) 78–84, https://doi.org/10.1016/j.micromeso.2005.11.023.
[40] A. Corma, M. Moliner, Á. Cantín, M.J. Díaz-Cabañas, J.L. Jordá, D. Zhang, J. Sun, K. Jansson, S. Hovmöller, X. Zou, Synthesis and structure of polymorph B of zeolite beta, Chem. Mater. 20 (2008) 3218–3223, https://doi.org/10.1021/CM8002244.
[41] M. Derewinski, J. Haber, J. Ptaszynski, J.A. Lercher, G. Rumplmayr, Acid-Base and Catalytic Properties of Alkali Metal Exchanged ZSM5, Stud. Surf. Sci. Catal. 28 (1986) 957–964, https://doi.org/10.1016/S0167-2991(09)60970-8.
[42] F. Güleç, O. Williams, E.T. Kostas, A. Samson, E. Lester, A comprehensive comparative study on the energy application of chars produced from different biomass feedstocks via hydrothermal conversion, pyrolysis, and torrefaction, Energy Convers. Manag. 270 (2022), 116260, https://doi.org/10.1016/J.ENCONMAN.2022.116260.
[43] M. Mohamadi-Baghmolaei, P. Zahedizadeh, A. Hajizadeh, S. Zendehboudi, Hydrogen production through catalytic supercritical water gasification: Energy and char formation assessment, Energy Convers. Manag. 268 (2022), 115922, https://doi.org/10.1016/J.ENCONMAN.2022.115922.
[44] P.A. Lazaridis, A.P. Fotopoulos, S.A. Karakoulia, K.S. Triantafyllidis, Catalytic fast pyrolysis of kraft lignin with conventional, mesoporous and nanosized ZSM-5 zeolite for the production of alkyl-phenols and aromatics, Front. Chem. 6 (2018), 295, https://doi.org/10.3389/fchem.2018.00295.
[45] Z. Ma, V. Custodis, J.A. Van Bokhoven, Selective deoxygenation of lignin during catalytic fast pyrolysis, Catal. Sci. Technol. 4 (2014) 766–772, https://doi.org/10.1039/c3cy00704a.
[46] A. Saraeian, S.J. Burkhow, D. Jing, E.A. Smith, B.H. Shanks, Catalyst Property Effects on Product Distribution during the Hydrodeoxygenation of Lignin Pyrolysis Vapors over MoO_3/γ-Al_2O_3, ACS Sustain. Chem. Eng. 9 (2021) 6685–6696, https://doi.org/10.1021/acssuschemeng.1c00295.
[47] H. Hernando, I. Moreno, J. Fermoso, C. Ochoa-Hernández, P. Pizarro, J. M. Coronado, D.P. Serrano, Biomass catalytic fast pyrolysis over hierarchical ZSM-5 and Beta zeolites modified with Mg and Zn oxides, Bioresour. Technol. 7 (2017) 289–304, https://doi.org/10.1007/s13399-017-0266-6.
[48] J. Fermoso, H. Hernando, P. Jana, I. Moreno, J. Přech, C. Ochoa-Hernández, P. Pizarro, J.M. Coronado, J. Čejka, D.P. Serrano, Lamellar and pillared ZSM-5 zeolites modified with MgO and ZnO for catalytic fast-pyrolysis of eucalyptus woodchips, Catal. Today 277 (2016) 171–181, https://doi.org/10.1016/j.cattod.2015.12.009.
[49] J. Fermoso, P. Pizarro, J.M. Coronado, D.P. Serrano, Advanced biofuels production by upgrading of pyrolysis bio-oil, Adv. Rev. 6 (2017) 1–18, https://doi.org/10.1002/wene.245.
[50] N. Priharto, S. Ghysels, M. Pala, W. Opsomer, F. Ronsse, G. Yildiz, H.J. Heeres, P. J. Deuss, W. Prins, Ex Situ Catalytic Fast Pyrolysis of Lignin-Rich Digested Stillage over Na/ZSM-5, H/ZSM-5, and Fe/ZSM-5, Energy Fuels 34 (2020) 12710–12723, https://doi.org/10.1021/acs.energyfuels.0c02390.
[51] S. Wang, Y. Jiao, Z. Li, Z. Wan, Y. Han, W. Yi, Modulating the acidity and accessibility of HZSM-5@Al-KIT-6 catalysts for the tandem catalytic upgrading of lignin pyrolysis vapors, Appl. Catal. A Gen. 656 (2023), 119129, https://doi.org/10.1016/J.APCATA.2023.119129.
[52] C. Auepattana-aumrung, K. Suriye, B. Jongsomjit, J. Panpranot, P. Praserthdam, Inhibition effect of Na+ form in ZSM-5 zeolite on hydrogen transfer reaction via 1-butene cracking, Catal. Today 358 (2020) 237–245, https://doi.org/10.1016/j.cattod.2019.08.012.
[53] H. Hernando, G. Gómez-Pozuelo, J.A. Botas, D.P. Serrano, Evaluating fractional pyrolysis for bio-oil speciation into holocellulose and lignin derived compounds, J. Anal. Appl. Pyrolysis 154 (2021), 105019, https://doi.org/10.1016/J.JAAP.2021.105019.
[54] E. Yaman, A.S. Yargic, N. Ozbay, B.B. Uzun, K.G. Kalogiannis, S.D. Stefanidis, E. P. Pachatouridou, E.F. Iliopoulou, A.A. Lappas, Catalytic upgrading of pyrolysis vapours: Effect of catalyst support and metal type on phenolic content of bio-oil, J. Clean. Prod. 185 (2018) 52–61, https://doi.org/10.1016/J.JCLEPRO.2018.03.033.
[55] A.T. To, D.E. Resasco, Role of a phenolic pool in the conversion of m-cresol to aromatics over HY and HZSM-5 zeolites, Appl. Catal. A Gen. 487 (2014) 62–71, https://doi.org/10.1016/J.APCATA.2014.09.006.
[56] Y. Yu, X. Li, L. Su, Y. Zhang, Y. Wang, H. Zhang, The role of shape selectivity in catalytic fast pyrolysis of lignin with zeolite catalysts, Appl. Catal. A Gen. 447–448 (2012) 115–123, https://doi.org/10.1016/j.apcata.2012.09.012.
[57] B.G. Janesko, Acid-catalyzed hydrolysis of lignin β-O-4 linkages in ionic liquid solvents: a computational mechanistic study, Phys. Chem. Chem. Phys. 16 (2014) 5423–5433, https://doi.org/10.1039/C3CP53836B.
[58] D.R. Naron, F.X. Collard, L. Tyhoda, J.F. Görgens, Production of phenols from pyrolysis of sugarcane bagasse lignin: catalyst screening using thermogravimetric analysis – Thermal desorption – Gas chromatography – Mass spectroscopy, J. Anal. Appl. Pyrolysis 138 (2019) 120–131, https://doi.org/10.1016/J.JAAP.2018.12.015.
[59] L.J. Ogbadu, PRESERVATIVES | Traditional Preservatives – Wood Smoke, Encycl. Food Microbiol. Second Ed. (2014) 141–148, https://doi.org/10.1016/B978-0-12-384730-0.00261-5.